



# Floor Failure Characteristics of Thick Coal Seam Mining Above Confined Aquifer

Tuan He<sup>1,2,3</sup> · Guo-dong Li<sup>3</sup> · Chuang Sun<sup>4</sup> · Feng Luo<sup>3</sup> · Xue-qing Li<sup>3</sup>

Received: 14 August 2021 / Accepted: 17 May 2022 / Published online: 8 June 2022  
© Society for Mining, Metallurgy & Exploration Inc. 2022

## Abstract

The mining-induced failure of the coal seam floor is essential for water inrush. The mining disturbance to the floor, especially in the thick coal seam, is severe, and the water inrush risk is also higher than that in regular thick coal seam excavation. The superposition of many stresses, including in situ stress, mining-induced stress, and confined water pressure, must be considered in the prediction of the floor failure depth. This study adopted the elasticity analysis, FLAC3D numerical simulation, and on-site acoustic wave test comprehensively. The thick coal seam working face of the Zhong-Yu coal mine affected by confined water was selected as the engineering background to study the characteristics of the floor failure. Based on elastic foundation theory and the superposition principle, the mechanical model and the failure depth criterion of the floor were established, respectively. The distribution and evolution of mining-induced stress and the plastic zone in surrounding rock during the mining process are obtained by FLAC3D. In addition, the changes in the P-wave wave velocity in the floor before and after mining were compared and studied by the acoustic wave test method. The range of floor damage depth is determined on the basis of the above research.

**Keywords** Thick coal seam mining · Confined water · Fully mechanized caving mining · Stress distribution · Floor failure depth

## 1 Introduction

Floor water inrush refers to a mine disaster in which the floor is damaged by mining, and the confined water flows into the mining space through the cracks and large areas, thereby resulting in a sharp increase in water inrush [1]. Coal mines in central and eastern China are seriously threatened by confined karst aquifers, especially the Ordovician limestone aquifers [2, 3]. The potential risk of water inrush from the floor has

dramatically endangered miners' lives and has become a danger in the development of coal mine projects.

Underground excavation causes pressure relief and redistribution of stress and the failure in surrounding rock. It also generates a certain depth of damaged area in the floor, which is the direct reason for floor water inrush [4]. The floor water inrush is caused by the combined action of mining stress evolution, floor failure, and upward flow of confined water [5, 6]. Many factors, such as the in situ and mining-induced stresses, the water pressure and amount of the aquifer, the thickness of the water-resisting layer, the evolution of the mining-induced fracture in the floor, and the geological structure, affect the floor water inrush [6]. Analyzing the balanced relationship among the influencing factors can predict the risk of floor water inrush. The water inrush coefficient theory is a widely used theory for evaluating the floor inrush risks [7–10]. In this theory, the stress–damage coupling analysis is often used. The initiation and development of fracture and damage are also introduced to determine floor permeability and damage. The “three-zone theory of floor” corresponds to another primary method for analyzing floor water inrush [11, 12]. According to this theory, the floor can be

✉ Guo-dong Li  
gd.li@cqu.edu.cn

<sup>1</sup> China Coal Research Institute, Beijing 100013, China

<sup>2</sup> State Key Laboratory of Coal Resources in Western China, University of Science and Technology, Xi'an 710054, China

<sup>3</sup> Hebei University of Engineering, Handan 056038, Hebei, China

<sup>4</sup> State Key Laboratory of Deep Geotechnical Mechanics and Underground Engineering, China University of Mining and Technology (Beijing), Beijing 100083, China

divided into three areas in terms of damage status similar to the roof. From top to bottom in the vertical direction, these areas are failure zone, intact zone, and upward flow zone [7, 13–15]. The failure zone is mainly caused by pressure relief, and the water pressure and mining-induced stress produce the upward flow zone. Water inrush occurs when the span of the upward flow zone and the failure zone overlap, or the water-resisting layer is wholly destroyed. Thus, the change in the floor failure depth and the extent of the upward flow zone during the mining process is the key to predicting the floor water inrush [16–20].

This study is based on the geological and mining conditions of the Zhong-Yu coal mine threatened by floor karst confined water. The combined theoretical modeling, numerical simulation, and sound wave field testing were used to study the distribution and evolution of the mining-induced stress and damaged zone in the floor.

## 2 Floor Stress Distribution Analysis Based on Elastic Foundation Theory

### 2.1 Geological Conditions of Coal Mines

Zhong-Yu coal mine mainly excavates the #3 coal seam with a height of 4.67 m which is a thick coal seam. It is a general coal mine located in Shanxi Province in Central China. The stratigraphic column in the vicinity of the seam is shown in Table 1. The No. 2308 working face refers to a fully mechanized mining face in the #3 coal seam with an average overburden depth of 438 m. The width and height of this mining face are 175 m and 5 m, and the panel length is 1133 m. Below the #3 coal seam, in the limestone layer approximately 13 m away, some areas contain confined water, and the maximum water pressure is about 0.3 MPa.

### 2.2 Establishment of Mechanics Model

According to the movement law of the overlying strata in underground mining [21], the roof behind the working face collapses after extracting the coal seam. The overburdened strata bend and compress the crumpled rock mass in the mined-out area with the advancing of the mining face. This process forms the compacted zone in the goaf (area A in Fig. 1). The stress in the floor between the working face and the compacted zone, which is the insufficiently compacted zone (area B), is released. The stress concentration in front of the working face (area C) is generated by the weight overlying the strata. The stress in the coal and rock mass beyond the mining influence is in situ stress (area D). With the continuous advancements of the working face, the floor experiences the effects of in situ stress, the concentrated stress ahead of the working face, and the compaction stress in the goaf successively.

Based on the theory of beams on the elastic foundation [22], the coal seam floor is regarded as a semi-infinite panel. The internal stress distribution of the floor is the same when subjected to uniform load, triangular load, and trapezoidal load with the same mean value, respectively. A mechanical model can be established in light of the general distribution of mining-induced stress (Fig. 2). Accordingly, the stress component at any depth below the floor can be obtained through subsequent analysis.

1. The range of the concentrated stress  $q_1$  in front of the working face is 0 to  $c$ , and the peak value is  $n\gamma h$ .  $q_1$  can be simplified into a uniform load, which can be calculated as follows:

$$q_1(x) = \frac{(n+1)\gamma H}{2}$$

**Table 1** The stratigraphic column near the coal seam at the Zhong-Yu coal mine

Lithology	Lithology description	Layer thickness
Mudstone	Gray-black, massive, conchoidal fracture, soft	0.56 m
Sandy mudstone	Gray-black, massive, soft, containing plant fossil fragments	5.22 m
# 3 coal seam	Black, developed endogenous fissures, metallic luster	4.67 m
Mudstone	Black, thin-layered, horizontal fissures are developed	1.00 m
Fine sandstone	Gray, layered, mainly composed of quartz, filled with mud	1.15 m
Mudstone	Gray-black, massive, flat fracture, soft	3.09 m
Fine sandstone	Gray, layered, mainly composed of quartz, cemented clay	1.74 m
Sandy mudstone	Gray, thin-layered, with broken core, sandwiched with 2 layers of siderite nodules with a thickness of 0.10 m	5.01 m
Limestone	Gray, medium-thick layered, cryptocrystalline structure, hard, broken core, developed fissures, and calcite film on the crevices	3.14 m

**Fig. 1** The sketch of the movement of the overlying strata in underground mining

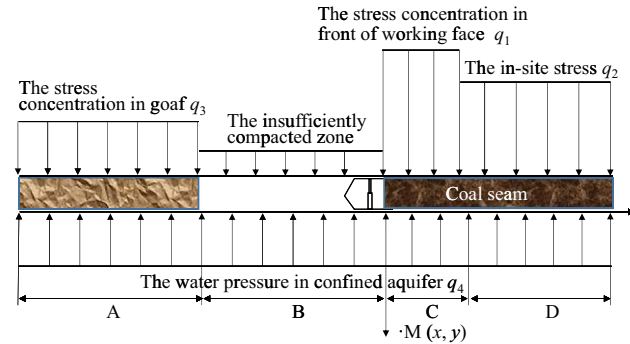
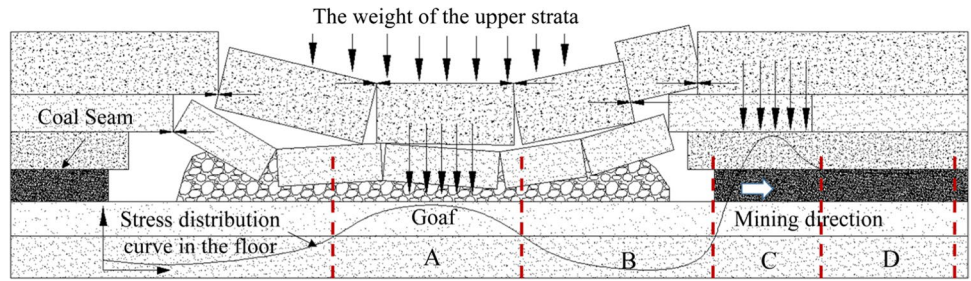


**Fig. 2** The mechanical model of stress distribution in the floor

At point M in the floor, the stress components  $\sigma_x^1$ ,  $\sigma_y^1$ , and  $\tau_{xy}^1$  formed by  $q_1$  can be calculated by the following equations:

$$\sigma_x^1 = \frac{(n+1)\gamma Hy}{2\pi} \left[ \frac{-c+x}{(c-x)^2+y^2} - \frac{x}{x^2+y^2} + \frac{\arctan\left(\frac{c-x}{y}\right) + \arctan\left(\frac{x}{y}\right)}{y} \right] \quad (1)$$

$$\sigma_y^1 = \frac{(n+1)\gamma H}{2\pi} \left[ \frac{(c-x)y}{(c-x)^2+y^2} + \frac{xy}{x^2+y^2} + \arctan\left(\frac{c-x}{y}\right) + \arctan\left(\frac{x}{y}\right) \right] \quad (2)$$

$$\tau_{xy}^1 = \frac{(n+1)\gamma Hy^2}{2\pi} \left[ \frac{1}{(c-x)^2+y^2} - \frac{1}{x^2+y^2} \right] \quad (3)$$

where  $(x, y)$  is the coordinate of M;  $\gamma$  is the average bulk density of the overlying strata,  $\text{kN/m}^3$ ;  $n$  is the stress concentration factor;  $H$  is the overburden depth, m;  $a, b, c,$  and  $d$  are the span of the compacted area in goaf, insufficiently compacted area, stress concentrated area, and in situ stress area in front of working face, m, respectively.

2. Based on the in situ stress, the stress in the floor can be calculated by the equation below:

$$q_2(x) = \gamma H$$

The stress components  $\sigma_x^2$ ,  $\sigma_y^2$ , and  $\tau_{xy}^2$  formed at point M in situ stress by  $q_2$  can be calculated by the following equations:

$$\sigma_x^2 = \frac{\gamma Hy}{\pi} \left[ \frac{c-x}{(c-x)^2+y^2} - \frac{c+d-x}{(c+d-x)^2+y^2} - \frac{\arctan\left(\frac{c-x}{y}\right)}{y} + \frac{\arctan\left(\frac{c+d-x}{y}\right)}{y} \right] \quad (4)$$

$$\sigma_y^2 = \frac{\gamma H}{\pi} \left[ \frac{(-c+x)y}{(c-x)^2+y^2} + \frac{(c+d-x)y}{(c+d-x)^2+y^2} \arctan\left(\frac{c+d-x}{y}\right) + \arctan\left(\frac{-c+x}{y}\right) \right] \quad (5)$$

$$\tau_{xy}^2 = -\frac{b(2c+d-2x)\gamma Hy^2}{\pi[(c-x)^2+y^2](c+d-x)^2+y^2} \quad (6)$$

3. In the compaction zone  $(-a-b < x < -b)$ , the weight of the overlying rock layer acts on the goaf floor. The stress in this area is  $q_3(x) = \gamma H$ . The stress components, namely,  $\sigma_x^3$ ,  $\sigma_y^3$ , and  $\tau_{xy}^3$ , formed by  $q_3$  at point M can be calculated by the following equations.

$$\sigma_x^3 = \frac{\gamma H}{\pi} \left( \arctan\left(\frac{a+b+x}{y}\right) - \arctan\left(\frac{b+x}{y}\right) \right) + \frac{y\gamma H}{\pi} \left[ \frac{b+x}{(x+b)^2+y^2} - \frac{a+b+x}{(x+a+b)^2+y^2} \right] \quad (7)$$

$$\sigma_y^3 = \frac{\gamma H}{\pi} \left( \arctan\left(\frac{a+b+x}{y}\right) - \arctan\left(\frac{b+x}{y}\right) \right) - \frac{y\gamma H}{\pi} \left[ \frac{b+x}{(x+b)^2+y^2} - \frac{a+b+x}{(x+a+b)^2+y^2} \right] \quad (8)$$

$$\tau_{xy}^3 = \frac{y^2\gamma H}{\pi} \left[ \frac{b+x}{(x+b)^2+y^2} - \frac{a+b+x}{(x+a+b)^2+y^2} \right] \quad (9)$$

4. The water pressure  $q_4$  of the pressurized water exerts pressure on the floor and acts on the whole mining process. The distribution of  $q_4$  in the floor is relatively uniform, which is  $q_4(x) = q(-a - b < x < c + d)$ . The stress components  $\sigma_x^4$ ,  $\sigma_y^4$ , and  $\tau_{xy}^4$  formed by  $q_4$  at point M can be calculated by the following equations:

$$\sigma_x^4 = \frac{q}{\pi} \left( \arctan \frac{a+b+x}{y} + \arctan \frac{c+d-x}{y} \right) - \frac{qy}{\pi} \left[ \frac{c+d-x}{(x-c-d)^2+y^2} + \frac{a+b+x}{(x+b+a)^2+y^2} \right] \tag{10}$$

$$\sigma_y^4 = \frac{q}{\pi} \left( \arctan \frac{a+b+x}{y} + \arctan \frac{c+d-x}{y} \right) + \frac{qy}{\pi} \left[ \frac{c+d-x}{(x-c-d)^2+y^2} + \frac{a+b+x}{(x+a+b)^2+y^2} \right] \tag{11}$$

$$\tau_{xy}^4 = \frac{y^2q}{\pi} \left[ \frac{1}{(x-c-d)^2+y^2} - \frac{1}{(x+b+a)^2+y^2} \right] \tag{12}$$

According to the superposition principle of elasticity [23], the stress component generated by the external loads at point M in the floor can be obtained as follows:

$$\begin{aligned} \sigma_x &= \sigma_x^1 + \sigma_x^2 + \sigma_x^3 + \sigma_x^4 \\ \sigma_y &= \sigma_y^1 + \sigma_y^2 + \sigma_y^3 + \sigma_y^4 \\ \tau_{xy} &= \tau_{xy}^1 + \tau_{xy}^2 + \tau_{xy}^3 + \tau_{xy}^4 \end{aligned} \tag{13}$$

The principal stress at this point can be obtained by substituting the stress components of point M into Eq. (13).

### 2.3 Analytical Distribution of Stress in the Floor

In terms of the working face’s mining and geological conditions, each parameter’s values are  $n = 2.2$ ,  $H = 400$  m,  $a = 70$  m,  $b = 1000$  m,  $c = 30$  m,  $d = 100$  m,  $p = 0.3$ , and  $\gamma = 26.69$  kN/m. The three-dimensional distribution of stresses in the floor can be obtained by calculations (Figs. 3a and 4a). In addition, the stress distribution below the working face ( $x = 0$ ) can also be drawn (Figs. 3b and 4b).

The floor failure mainly occurs near the excavated area at a certain depth. The floor damage decreases with the added overburden depth, whereas the bearing capacity and stress concentration increase. Stress gradually reduces in surrounding rocks beyond the failure zone. Figures 3a and 4a show that the stress in the floor near the working face changes dramatically. Due to pressure relief, the stress in the insufficient area near the working face is lower than those in other areas. The floor in front of the working face is subjected to the overlying strata weight load transmitted by the coal wall, and the stress concentration increases. When the distance to the working face extends, the shear and vertical stress changes tend to slow down at the same depth. On the contrary, the shear and vertical stresses slowly rise horizontally in the floor.

### 2.4 Floor Failure Depth Criterion

Establishing the criterion to identify the failure depth of the floor is an essential basis for predicting the risk of confined water inrush. When it transitions from the elastic zone to the plastic area in the floor, the principal stress of the rock mass should meet the limit equilibrium

**Fig. 3** The distribution of shear stress in the floor. **a** Three-dimensional distribution. **b**  $x = 0$

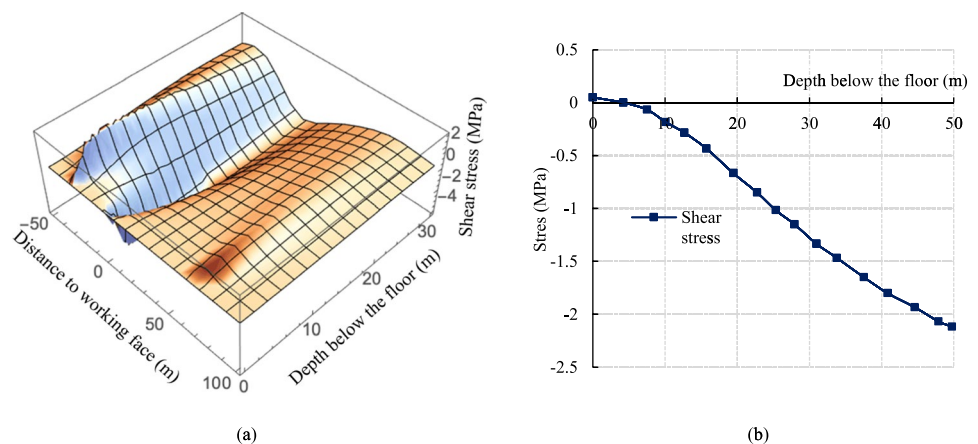
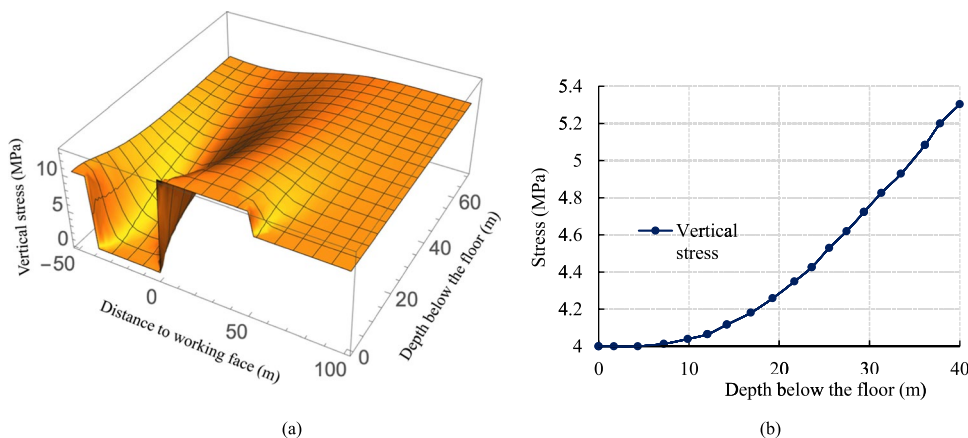


**Fig. 4** The distribution of vertical stress in the floor. **a** Three-dimensional distribution. **b**  $x=0$



condition. Based on the Mohr–Coulomb failure criterion, Eq. (15), which is based on the maximum and minimum principal stresses,  $\sigma_1$  and  $\sigma_3$  can be used to calculate the failure depth of the floor.

$$\frac{1 + \sin \varphi}{1 - \sin \varphi} \sigma_3 + \frac{2c \cos \varphi}{1 - \sin \varphi} < \sigma_1 \tag{15}$$

According to the calculation model and criterion of the principal stress established by Eqs. (13–14), the theoretical value  $\sigma_{1t}$  and the limit value  $\sigma_{1c}$  distribution of  $\sigma_1$  at different depths of the floor can be calculated, respectively (Fig. 5). When  $\sigma_{1t} > \sigma_{1c}$ ,  $\sigma_1$  in the surrounding rock of the floor is larger than the strength, thereby causing damage. When the depth below the floor is 9.2 m, the curves of  $\sigma_{1t}$  and  $\sigma_{1c}$  intersect. This finding indicates that the stress at this point is equal to its strength, which is a critical point of instability. When the floor depth is less than 5 m,  $\sigma_{1t}$  is more significant than  $\sigma_{1c}$ , and the surrounding rock of the floor is completely damaged. This area can be named a severely damaged area. When the depth is from 5 to 9.2 m, it corresponds to the less damaged zone. When the depth is greater than 9.2 m, the rock mass bearing capacity can withstand the maximum principal stress ( $\sigma_{1t} < \sigma_{1c}$ ). The floor is in a complete state. Therefore, the damage depth of the floor of No. 2308 working face is 9.2 m.

### 3 Distribution and Evolution of Mining Stress and Plastic Zone in the Floor

#### 3.1 Establishment of Numerical Model

This simulation focuses on the stress and damage changes in the floor. FLAC3D is used in this simulation.

The numerical model is established on the basis of the geological and mining conditions of No. 2308 working face. The thickness of the roof and floor of the coal seam are 68 m and 72 m, respectively. The model’s length, width, and height are 500, 300, and 170 m, respectively (Fig. 6). The overburden depth of the coal seam is 400 m. The weight of the overlying strata is replaced by applying boundary stress to reduce the number of zones in the model and shorten the calculation time. According to the average bulk density of the overlying strata and the overburden depth, the stress applied on the top of the model is 8.3 MPa. The bottom boundary of the model adopts the displacement constraint in the vertical direction, and the lateral boundary imposes the displacement constraint in the horizontal direction. In addition, zones with a width of 50 m are generated on the four sides of the mining panel to reduce the influence of boundary effects on the

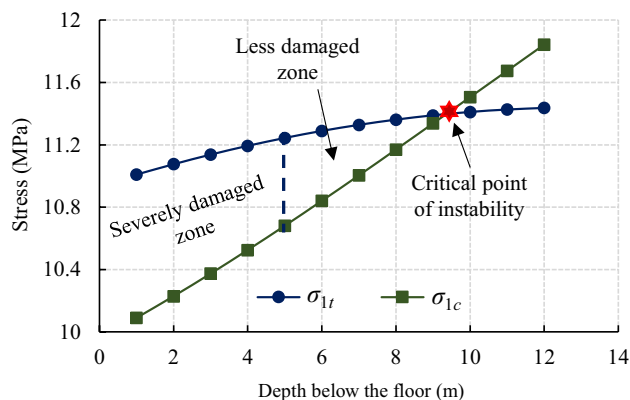
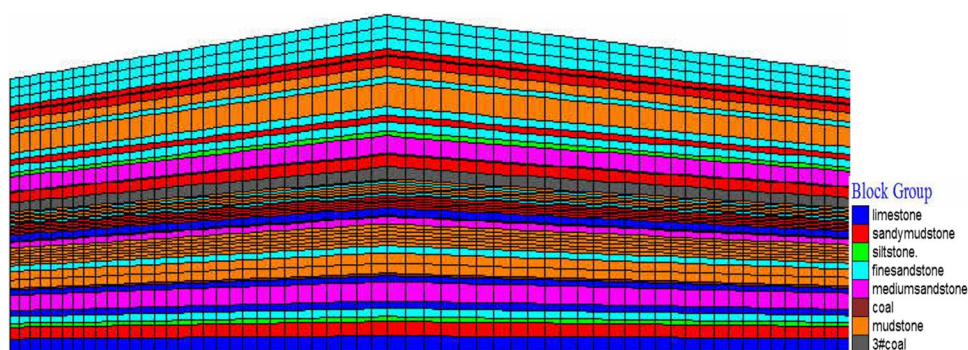


**Fig. 5** The distribution of  $\sigma_{1t}$  and  $\sigma_{1c}$  in the floor

**Fig. 6** The numerical model of No. 2308 working face



stress distribution. The total advancing distance of the working face is 120 m.

The deformation and failure of the rock strata in the model follow the Mohr–Coulomb criterion. According to the mechanical test results [24], the mechanical parameter values of each lithology that appears in the model are shown in Table 2.

### 3.2 Distribution of Plastic Zone

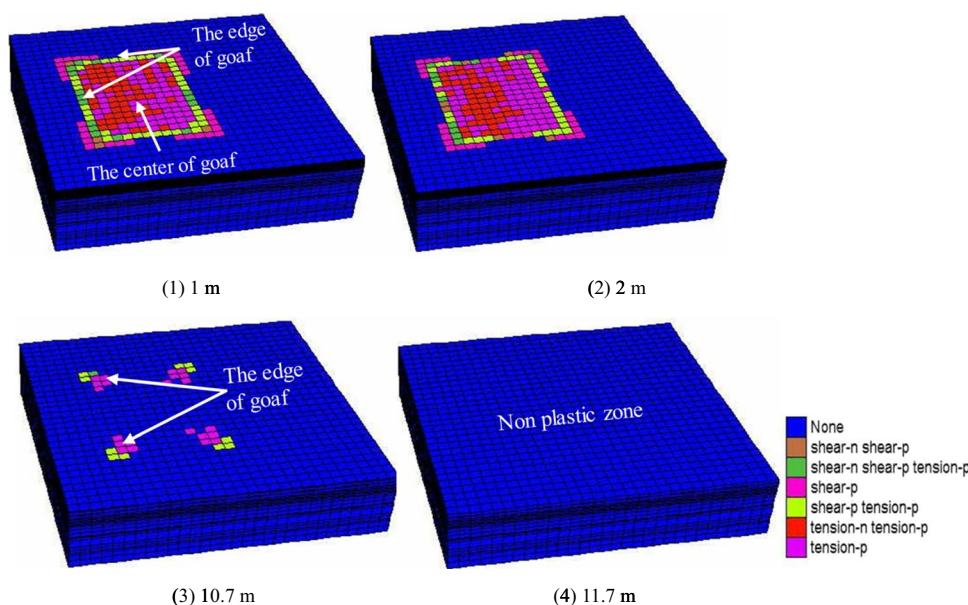
Figure 7 shows the horizontal section of the plastic zone at different overburden depths ( $h = 1\text{ m}, 2\text{ m}, 10.7\text{ m}$ ,

11.7 m) in the floor. The floor within 2 m is seriously damaged. In this area, the central part of the goaf is mainly a tensile failure, whereas the surrounding area is a predominantly tensile and shear mixed failure. For the floor 10.7 m away from the coal seam, only the rock mass at the four corners of the goaf exhibited shear failure, and the middle of the goaf is still in the elastic state. Therefore, the failure depth of the floor at the side of the excavated area is the largest, especially for the corners of the mining panel. Consequently, the probability of floor water inrush in these areas is high.

**Table 2** The value of mechanical parameters of each lithology in the simulation

Lithology	Cohesion (MPa)	Friction angle (°)	Shear modulus (MPa)	Bulk modulus (MPa)	Density (kg/m. <sup>3</sup> )	Tensile strength (MPa)
Mudstone	2.52	25	980	840	2560	1.93
Limestone	3.89	30	1411	1044	2300	2.76
Sandy mudstone	2.80	31	830	790	2100	2.20
Coal	1.75	20	673	530	1450	1.22
Fine sandstone	5.21	29	1783	1588	2210	3.47

**Fig. 7** The distribution of the plastic zone in the floor. (1) 1 m. (2) 2 m. (3) 10.7 m. (4) 11.7 m



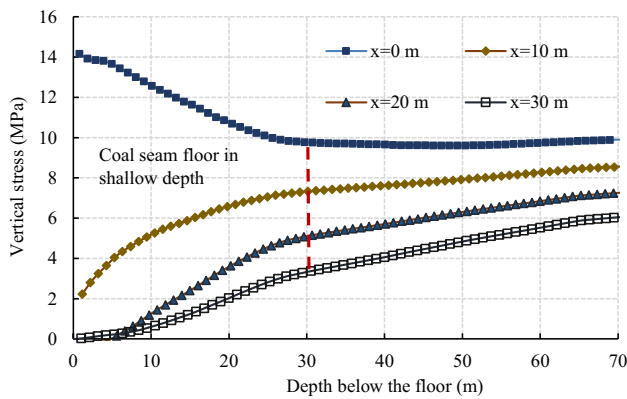


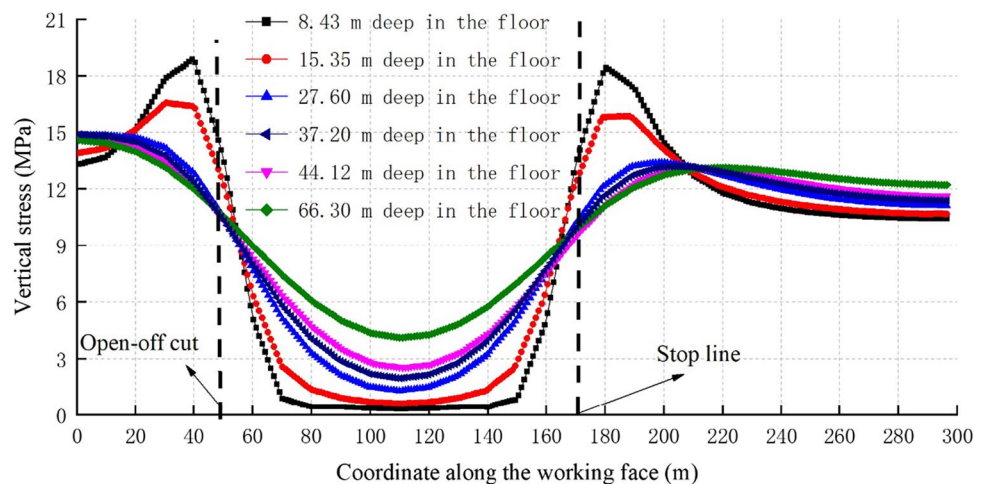
Fig. 8 The stress distribution below the floor

### 3.3 Stress Distribution

The high-stress concentration indicates that the floor has a strong bearing capacity and good integrity. Along the coal seam strike, the vertical stress distribution in the floor at the distances of 0, 10, 20, and 30 m away behind the working face can be extracted (Fig. 8). The stress of the shallow floor under the coal wall ( $x=0$ ) is higher, whereas the floor in the goaf behind the working face has low stress in the shallow part. Moreover, when  $x > 20$  m, the pressure relief of the shallow floor is sufficient. When the burying exceeds 30 m, the stress in the floor gradually recovers to the in situ stress.

The stress distribution in the floor at different depths below the working face is shown in Fig. 9. When the depth is less than 27.6 m, the stress concentration of the floor is higher, and the damage is relatively lower than in other areas. The peak stress in front of the working face is approximately 10 m. Therefore, the plastic zone formed in the coal wall and floor ahead of the working face is 10 m. When the depth is larger than 27.6 m, the stress concentration in front of the working face decreases significantly, and the floor failure also declines.

Fig. 9 The stress distribution of the floor at different depths along the advancing direction of the working face



## 4 Acoustic Testing of the Floor Failure Depth

### 4.1 Principle of Sonic Detection

The acoustic test method is used to test the floor failure depth of the No. 2308 working face in the Zhong-Yu coal mine to verify the theoretical and numerical results. The acoustic testing method detects the integrity of the surrounding rock by using the geometric and physical attenuations of the elastic wave when it propagates in the rock mass, and the propagation velocity has differences. Based on the boundary and initial conditions of a homogeneous and isotropic elastic half-space, the velocity of the longitudinal wave (P-wave) and shear wave (S-wave) can be solved by the following equations [25]:

$$V_p = \sqrt{\frac{E(1-\nu)}{\rho(1+\nu)(1-2\nu)}}$$

$$V_s = \sqrt{\frac{E}{2\rho(1+\nu)}}$$

where  $E$ ,  $\rho$ , and  $\nu$  correspond to the elastic modulus, density, and Poisson’s ratio of the material, respectively.

When the stress concentration is greater, the density of the rock mass is more significant, the damage is less, and the speed of the sound wave propagation is fast [26]. Hence, the range of the failure area can be obtained by measuring the P-wave velocity of the floor at different depths in the test borehole.

### 4.2 Test Equipment and Method

The equipment used in the test is RSM-SY5 (n) Digital Ultrasonic Instrument. It includes one ultrasonic transmitter and an analysis system (Fig. 10a), two receiving probes, one transmitting probe (Fig. 10b), and pushrods (Fig. 10c).

**Fig. 10** Components of RSM-SY5(N) Digital Ultrasonic Instrument. **a** Ultrasonic transmitter and analysis system. **b** One-transmitting dual-receiving probe. **c** Pushrods

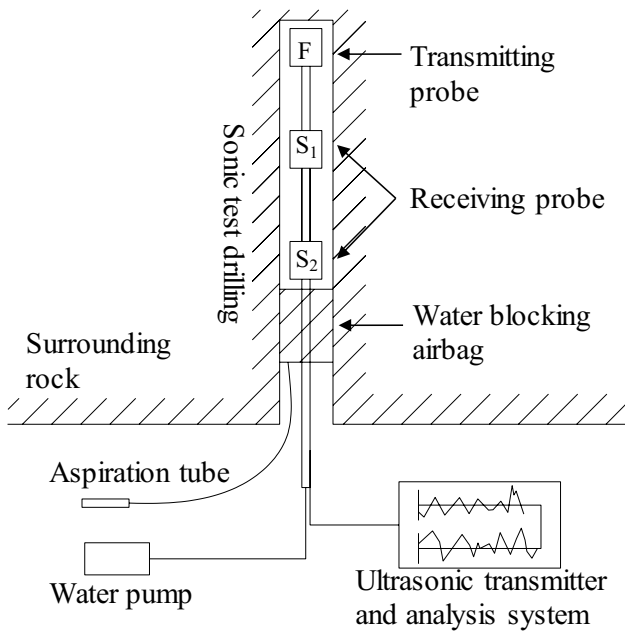
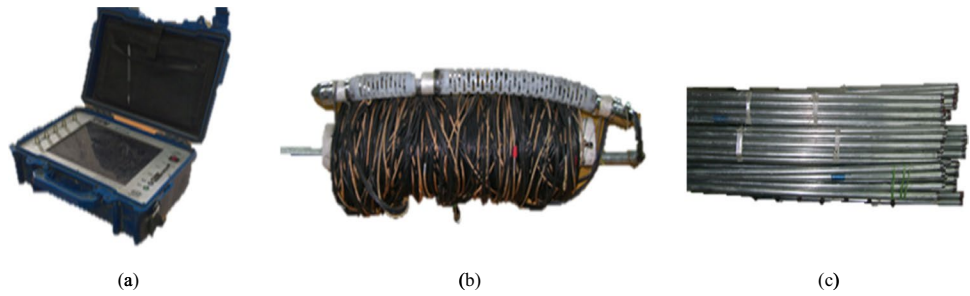


**Fig. 11** The layout of acoustic test

The layout of the receiving and transmitting probes in the test hole is shown in Fig. 11 [27].

The distance between the transmitting probe F and the two receiving probes,  $S_1$  and  $S_2$ , is  $L_1$  and  $L_2$ , respectively. The propagation time of the P-wave is  $T_1$  and  $T_2$ . Then, the velocity  $v_p$  of P-wave in the rock mass can be calculated by the following formula:

$$v_p = \frac{\Delta L}{\Delta T} = \frac{L_1 - L_2}{T_1 - T_2}$$

The test is conducted in the track transportation roadway of the working face, and two test boreholes with  $\Delta L = 8$  m in the floor are set. The K1 borehole is in front of the working face is 150, and the K2 behind the working face is 80 m. The two boreholes are parallel to each other to reduce the measurement error. The theoretical and numerical results of the failure depth of the floor are 9.2 m and 10.7 m, respectively.

Therefore, the borehole length in the field test is taken as 13 m. In addition, observation is carried out immediately after drilling construction to avoid hole collapse.

### 4.3 Test Results

Through acoustic testing, the variation of the P-wave velocity in the floor at different depths is shown in Fig. 12. The heterogeneity of the rock mass is the main factor that influences the accuracy of the results. When the floor rock mass homogeneity is low, the volatility is more fluctuating. The variation range of  $v_p$  is approximately 400 m/s.

Borehole K2 is not affected by mining, and the floor is still intact. The results indicate that as the depth deepens,  $v_p$  increases slightly from 2500 m/s at a depth of 5.5 m to 2900 m/s, which is 13 m deep in the floor. K2 is located behind the working face and has suffered mining influence. Within 9.5 m of the floor,  $v_p$  is lower than the result of the same depth of borehole K1. The  $v_p$  of the shallow rock mass in the K2 borehole is only 1700 m/s. When the depth exceeds 9.5 m,  $v_p$  in K2 is close to the result of K1. Therefore, the failure depth of the floor caused by mining is nearly 9.5 m. When the depth exceeds 9.5 m, the floor is unbroken. The results of theoretical analysis and field measurement are close to each other, and the numerical result is larger. Therefore, when the above methods are used to determine

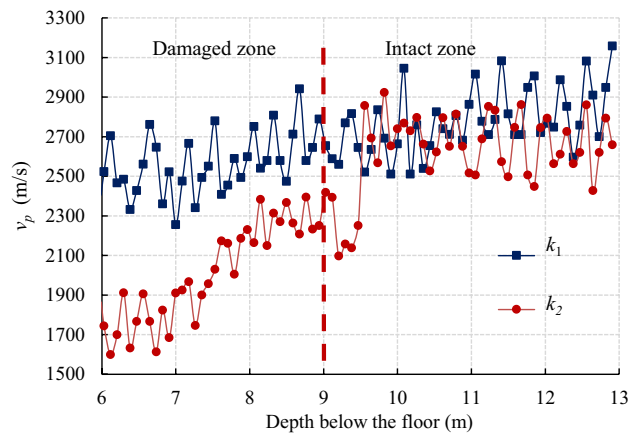


**Fig. 12** The acoustic test result in Zhong-Yu coal mine



the failure depth of the floor, the number of sampling and drilling holes should be increased to improve the accuracy of the test.

## 5 Conclusion

This study focuses on the floor damage depth of the fully mechanized working face of thick coal seams under the action of confined water. The No. 2308 working face of the Zhong-Yu coal mine is taken as the engineering object. Theoretical analysis, numerical simulation, and acoustic testing are used for comprehensive analysis. The mining-induced stress distribution and failure in the floor are investigated. The main conclusions are drawn as follows:

1. A mechanical model of the floor based on the superposition principle is established. In this model, the main loads applied on the floor are in situ stress, concentrated stress in front of working face, goaf compaction stress, and the water pressure generated by the confined water in the refined aquifer. Based on the elastic foundation theory, the distribution of principal stress in the floor is obtained, and the criterion of floor failure depth is established.
2. The numerical simulation shows that when the depth of the floor is less than 2 m, the surrounding rock is seriously damaged mainly by tensile failure. Tension-shear mixed failure primarily occurs around the goaf. When the depth is 10.7 m, only the surrounding rock at the four corners of the goaf is damaged by shearing. The stress concentration is higher at the shallow depth of the floor below the coal wall. When the distance behind the working face is higher than 20 m, the pressure relief of the shallow floor is sufficient. When the overburden depth exceeds 30 m, the stress in the floor gradually recovers to the in situ stress.
3. The acoustic field test shows that the P-wave velocity increases from 2500 to 2900 m/s within the depth of 5.5 to 10 m, but its value in the shallow floor is only 1700 m/s because of mining, and the failure depth of the floor in this working face is about 9.5 m deep.

**Funding** Support for this work was provided by the Natural Science Foundation of Hebei Province (E2020402042, E2020402041, E2021402061); open fund project of State Key Laboratory (SKLCKRF20-04); the NatiCoal Geology & Exploration Natural Science Foundation of China (51804093).

## Declarations

**Conflict of interest** The authors declare no competing interests.

## References

1. Zhai M, Bai H, Wu L, Wu G, Yan X, Ma D (2022) A reinforcement method of floor grouting in high-water pressure working face of coal mines: a case study in Luxi coal mine, North China. *Environ Earth Sci* 81(1):1–17
2. Feng L, Zhao GM, Meng XR (2011) Analysis calculation on floor failure law of coal mining above pressurized water strata and application. *Coal Sci Technol* 39(9):13–16
3. Zhang R, Jiang ZQ, Yu ZR, Cao DT, Wang ZS (2013) Comprehensive testing and numerical analysis on the failure characteristics of mining coal seam floor. *J Min Saf Eng* 30(4):531–537
4. Coleman PJ, Kerkering JC (2007) Measuring mining safety with injury statistics: lost workdays as indicators of risk. *J Safety Res* 38(5):523–533
5. Kuscer D (1991) Hydrological regime of the water inrush into the Kotredz coal mine (Slovenia, Yugoslavia). *Mine Water Environ* 10(1):93–101
6. Shi L, Singh RN (2001) Study of mine water inrush from floor strata through faults. *Mine Water Environ* 20(3):140–147
7. Odintsev VN, Miletenko NA (2015) Water inrush in mines as a consequence of spontaneous hydrofracture. *J Min Sci* 51(3):423–434
8. Polak K, Rózkowski K, Czaja P (2016) Causes and effects of uncontrolled water inrush into a decommissioned mine shaft. *Mine Water Environ* 35(2):128–135
9. LaMoreaux JW, Wu Q, Wanfang Z (2014) New development in theory and practice in mine water control in China. *Carbonates Evaporites* 29(2):141–145
10. Nguyen QP, Van Nguyen M, Konietzky H, Nguyen QL, Pham NA (2014) Numerical simulation of the influence of water inrush on underground coal mining stability in Vietnam. In: *Mine planning and equipment selection* (pp. 629–636). Springer, Cham
11. Guan Y, Li H, Lu J (2003) Research of No. 9 coal seam floor's fracture regularity in Xiandewang Coal Mine. *Mei T'an Hsueh Pao (Journal of China Coal Society)* 2:121–125
12. Zhu SY, Zhou HY, Li XF, Yang CW, Sun Q (2013) Deformation and failure mechanism of mining floor in “three-soft” coal seam based on field measurement. *J Min Saf Eng* 30(4):518–525
13. Zhang Y, Yang L (2021) A novel dynamic predictive method of water inrush from coal floor based on gated recurrent unit model. *Nat Hazards* 105(2):2027–2043
14. Bringemeier D (2012) Inrush and mine inundation—a real threat to Australian coal mines. In *Proceedings of the International Mine Water Association Annual Conference, Bunbury, Australia* (Vol. 30)
15. Dean CZXBCL, Jianzhong JFWQG (1996) The prediction model of ground water inrush from floor in jiaozuo coal mine. *Coal Geology and Exploration* 5:38–41
16. Bukowski P (2015) Evaluation of water hazard in hard coal mines in changing conditions of functioning of mining industry in Upper Silesian Coal Basin—USCB (Poland). *Arch Min Sci* 60(2):455–475
17. Mahdevari S, Shahriar K, Esfahanipour A (2014) Human health and safety risks management in underground coal mines using fuzzy TOPSIS. *Sci Total Environ* 488:85–99
18. Linkov AM (2013) Analytical solution of hydraulic fracture problem for a non-Newtonian fluid. *J Min Sci* 49(1):8–18
19. Zubkov VV, Koshelev VF, Lin’Kov, A. M. (2007) Numerical modeling of hydraulic fracture initiation and development. *J Min Sci* 43(1):40–56
20. Li G, Cao S, Luo F, Li Y, Wei Y (2018) Research on mining-induced deformation and stress, insights from physical modeling and theoretical analysis. *Arab J Geosci* 11(5):1–9

21. Yu YX, Huang RB, Wang BQ (2016) Analysis on limit equilibrium zone of coal pillar in mining roadway based on mechanical model of elastic foundation beam. *J Eng Mech* 142(4):04016009
22. Guo Z, Liu X, Zhu Z (2017) Elastic solution for a deep twin tunnel's stress based on complex variable theory and the superposition principle. *J Eng Res* 5(2):69–86
23. Liu Y, Ye Y, Wang Q, Liu X, Wang W (2019) Predicting the loose zone of roadway surrounding rock using wavelet relevance vector machine. *Appl Sci* 9(10):2064
24. Ulusay R (Ed.) (2014) *The ISRM suggested methods for rock characterization, testing and monitoring: 2007–2014*. Springer
25. Agliardi F, Sapigni M, Crosta GB (2016) Rock mass characterization by high-resolution sonic and GSI borehole logging. *Rock Mech Rock Eng* 49(11):4303–4318
26. He XQ, Zhou C, Song DZ, Li ZL, Cao AY, He SQ, Khan M (2021) Mechanism and monitoring and early warning technology for rockburst in coal mines. *Int J Miner Metall Mater* 28(7):1097–1111
27. Dai J, Yang F, Wu Y, Zou QQ (2014) Application of RSMSY5 (N) acoustic-waves-monitor in releasing zone measuring and test. *Coal Technol* 33(12):76–78

**Publisher's Note** Springer Nature remains neutral with regard to jurisdictional claims in published maps and institutional affiliations.